J Mater Sci (2007) 42:8215–8221
DOI 10.1007/s10853-007-1696-5

A novel method for producing open-cell Al_2O_3-ZrO_2 ceramic foams with controlled cell structure

Jing-yuan Yu · Xu-dong Sun · Qiang Li · Xiao-dong Li

Received: 1 November 2006 / Accepted: 15 March 2007 / Published online: 22 June 2007

Abstract A novel method was introduced to prepare open-cell Al_2O_3–ZrO_2 ceramic foams with controlled cell structure. This method used epispastic polystyrene (EPS) spheres to array ordered templates and centrifugal slip casting in the interstitial spaces of the EPS template to obtain cell struts with high packing density. Aqueous Al_2O_3–ZrO_2 slurries with up to 50 vol.% solid contents were prepared and centrifuged at acceleration of 2,860*g*. The effect of the solid contents of slurries on segregation phenomena of different particles and green compact uniformity were investigated. In multiphase system, the settling velocities of Al_2O_3 and ZrO_2 particles were calculated. Theory analysis and calculated results both indicated segregation phenomenon was hindered for slurries with 50 vol.% solid content. The cell struts of sintered products had high green density (61.5%TD), sintered density (99.1%TD) and homogeneous microstructures after sintered at 1,550 °C for 2 h. The cell size and porosity of Al_2O_3–ZrO_2 ceramic foams can be adjusted by changing the size of EPS spheres and the load applied on them during packing, respectively. When the porosity increased from 75.3% to 83.1%, the compressive strength decreases from 3.82 to 2.07 MPa.

J.-y. Yu (✉) · X.-d. Sun · Q. Li · X.-d. Li
Key Laboratory for Anisotropy and Texture of Materials (Ministry of Education), Northeastern University, Shenyang 110004, China
e-mail: yujingyuan1979@yahoo.com.cn

Q. Li
College of Materials & Chemical Engineering, Liaoning Institute of Technology, Jinzhou 121001, China

Introduction

Ceramic foams can be widely used in catalyst carriers, hot gas collectors, molten metal filters, chemical sensors and separation membranes [1, 2] because they have unique three-dimensional skeleton structure, high porosity, low density, high thermal stability and resistance to chemical attack [3, 4].

Alumina matrix ceramic foams with the special property of high resistance to molten aluminum attack are mainly used in filtering molten aluminum. The common preparation approach is the sponge method which involves immersion of a polymeric open-cell foam in ceramic slurry, pyrolysis of the organic matter and sintering at special temperature [5]. Alumina matrix foams produced by above process have low strength and fracture toughness due to high porosity and thin struts with holes, inducing them sensitive to structural stress and limit their application [6]. There have been some ways to improve their mechanical properties such as the addition of fibers to the ceramic structure [7]. It is, however, difficult to uniformly impregnate polymeric sponges with the ceramic slurry containing fibers. So a simple and efficient method is urgently required to improve the density of cell strut and achieve high strength.

In this paper, centrifugal slip casting into the interstitial spaces of pre-arrayed epispastic polystyrene (EPS) template was used to produce Al_2O_3–ZrO_2 ceramic foams. ZrO_2 particles with proper contents can improve mechanical properties of Al_2O_3 matrix foam because of t–m phase transformation of ZrO_2 particles [8]. The general procedure is as follows: forming a close-packed template with epispastic polystyrene (EPS) spheres, filling the interstitial spaces of the template with ceramic slurries by centrifugal slip casting, and removing the template to obtain a porous

inverse replica. Uniform cell structure and dense cell strut are acquired by this method. Additionally, cell size and porosity of Al_2O_3–ZrO_2 foams can be adjusted by changing the diameter of EPS spheres and load applied on them during packing, respectively. In above process, centrifugal slip casting can obtain optimal particle packing, minimal flaw size and good sintering behavior [9]. Though centrifugal slip casting can lead the drawback of mass segregation due to the difference of sizes and densities of starting powders, the drawback can be mostly avoided by adopting slurries with high solid contents [10]. In this paper, the effect of solid contents of slurries on green compact uniformity and the adjustment of cell structure were studied. Green and sintered density, sintering behavior, microstructure and compressive strength of the sintered products were investigated as well.

Experimental procedure

α-Al_2O_3 powder was used with 99.99% purity and an average particle size of 0.2 μm. ZrO_2 powder (TZ-3Y) had 99.5% purity and median diameter of 0.15 μm. Polycarboxylic ammonium with an average molecular weight of 10,000 was used as the dispersant. EPS spheres (in Fig. 1) were sieved by 14-mesh screen and then slowly put into the cylindrical mold in a layer-by-layer manner. When these spheres were stacked to definite height, a soft sponge was first placed on the top of EPS template in order to transmit the applied force and obtain uniform compaction. The stainless steel plates with fixed weight were then put on the top of the sponge one by one according to the demand for applied load. Finally, the whole mold was heated to 120 °C for 30 min to improve the linking strength between the spheres and preserve their deformation. The template was subsequently removed by pyrolysis method.

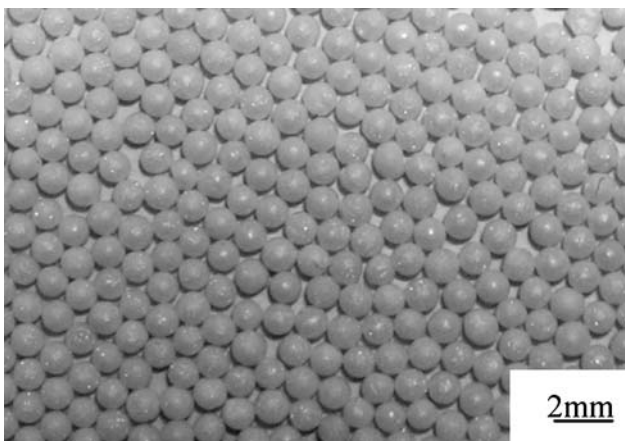

Fig. 1 A representative picture of EPS spheres

Figure 2 shows the flow chart of the centrifugal slip casting process. Two kinds of powders were mixed in a special proportion (Al_2O_3–15 vol.% ZrO_2), and then dispersed in distilled water by ball milling in a plastic pot for 24 h at 1 wt.% dispersant and pH 10. Aqueous suspensions with solid contents varying from 30 vol.% to 50 vol.% were prepared. The prepared slurries containing Al_2O_3 and ZrO_2 particles were poured into the interstitial spaces of the EPS template and then centrifuged at a centrifugal acceleration of 2,860g. After centrifugation, the specimens were removed from the mold and dried for 24 h at room temperature. In the dried compacts with a dimension of about φ40 mm × 40 mm, the green density variations of cell struts along the height of the compacts were investigated. Additionally, dried specimens were sintered in air at 1,550 °C for 2 h and detected linear shrinkage, sintered density, porosity, compressive strength. Green and sintered densities of Al_2O_3–ZrO_2 ceramic foams were measured by the Archimedes principle and their apparent morphology was observed by stereoscope(OLYMPUSSZ61). Microstructure of the specimens was analyzed using scanning electron microscopy (SSX-505) on their polished and thermally etched surfaces. Compressive strength was measured using a universal testing machine (CMT5105) with a loading rate of 0.5 mm/min, and the specimen size is φ 20 mm × 20 mm.

Results and discussion

Effect of applied loads on the EPS template

Figure 3 shows the height change of EPS template at different applied loads. The extent of change, i.e., $\psi = \Delta h/h_0$, where h_0 is the original height of the template and Δh is the height change. In Fig. 3, the height of the template gradually decreases with the increase of the applied loads. This is mainly due to the deformable nature of EPS spheres, which are compressed to dense packing at high load applied. Hence a higher packing density than that using hard particle such as salt can be achieved. With the increase of the deformation of EPS spheres, the porosity of the templates decreases.

Effect of solid contents of slurries on green compact uniformity

In order to observe density uniformity of cell struts in the specimens and define the limits of hindered mass segregation, slurries with different solid contents from 30 vol.% to 50 vol.% were cast at 2860G for 90min. The dried samples were sectioned to 4 cakes about 10 mm thick to

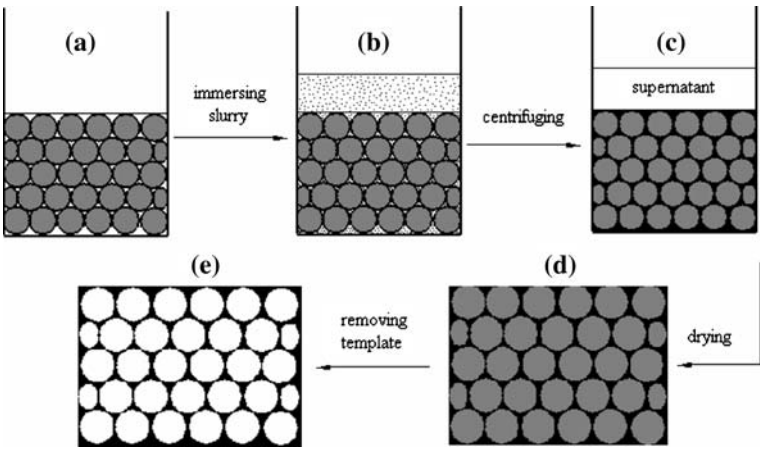

Fig. 2 Flow chart of centrifugal slip casting process

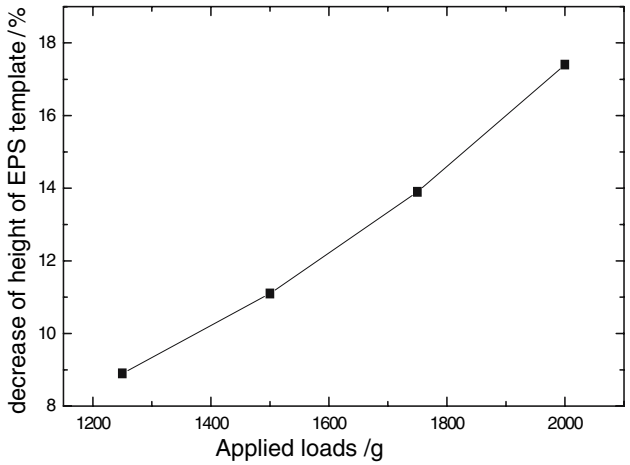

Fig. 3 Effect of applied loads on the change of the height of EPS template

determine green densities of cell struts. These green densities are summarized in Table 1. As can be seen in Table 1, green density in top cell struts is lower than that closer to the bottom of the cakes. With the decrease of the solid contents, the density difference in the top and bottom increases. However, the difference is negligible for all parts that were consolidated from slurries with 50 vol.% solid content because of the increase of viscosity. In the slurries with high solid content, the number of particles increases and the distance between particles decreases, improving the interactional force of particles and making it difficult for a particle to pass through the neighboring particles under a centrifugal force field. So obvious segregation phenomena are effectively hindered.

Table 1 Green density of cell struts in cakes prepared with slurries of various solid content

Slurries (vol.%)	Green density(%)			
	Cake 1	Cake 2	Cake 3	Cake 4
30	58.3	59.2	60.7	61.1
40	58.8	59.5	60.4	61.0
50	60.7	61.1	61.4	61.5

Segregation phenomena in a multiphase system are more complex than that in monolithic system because size and density difference of various particles can result in both mass and phase segregation. The larger and heavier particles incline to accumulate at the bottom of samples but the smaller and lighter particles tend to coagulate at the top, which leads segregation with different degree. Segregation essentially derives from different settling velocities of multifarious particle in a suspension, which has been well investigated by experimentally [11] and theoretically [12]. The basic principles of sedimentation originate from Stokes' Law, which describes the moving of a sphere in an infinite medium. In this paper, the movement of slurries in the template still followed creeping flow conditions because its Reynolds numbers (= $2\rho_L v a \eta^{-1}$) was below 1. The Reynolds number can be calculated with the data from Table 2 and with the use of Eq. 6. Due to creeping flow, the friction F_f exerted on a single sphere can still be described according to Stokes' Law [13]:

$$F_f = -6\pi\eta a v(t) \tag{1}$$

In a centrifugal force field, the total forces exerted on the particles are simplified as centrifugal force (F_c), buoyant force (F_b), and frictional force (F_f). Figure 4 shows sketch map of the forces exerted on the particles in a suspension. The forces are described as follows:

$$F_c = \frac{4}{3}\pi a^3 \rho_p r\omega^2 \tag{2}$$

$$F_b = \frac{4}{3}\pi a^3 \rho_L r\omega^2 \tag{3}$$

Table 2 Parameters and data used by this paper

Parameter	Value
r	0.09 m
ω	418.7 rad/s
d_1	0.2 μm
d_2	0.15 μm
η	1.8×10^{-3} pa s
ρ_1	3,940 kg/m^3
ρ_2	6,050 kg/m^3
ρ_L	1,000 kg/m^3
$n_1 = n_2$	4.65

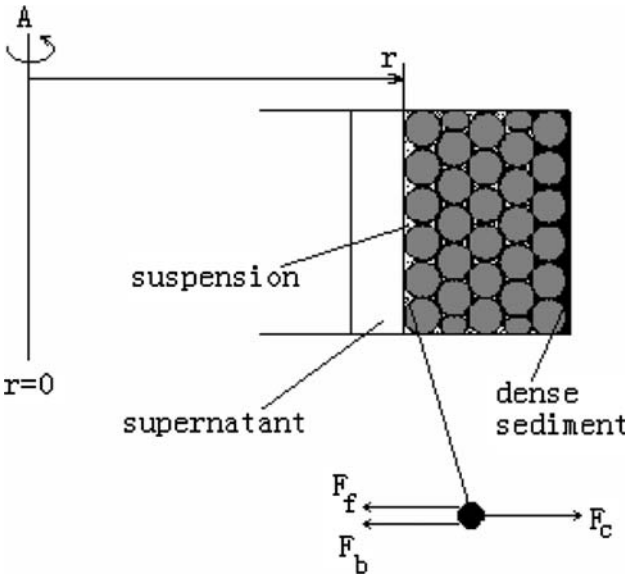

Fig. 4 Schematic of the forces on the particle in suspensions during centrifugal process

where η is liquid viscosity, a is particle radius, ρ_p is particle density, ρ_L is liquid density, ω is angular velocity, and r is radial coordinate.

In monolithic system, the following second-order differential equation is obtained to describe the particle movement using Newton's second law:

$$\frac{4}{3}\pi a^3(\rho_p - \rho_L)r\omega^2 - 6\pi\eta a\frac{dr}{dt} = \frac{4}{3}\pi a^3\rho_p\frac{d^2r}{dt^2} \quad (4)$$

Integration of Eq. 4 over time t results in:

$$v(t) = \frac{2a^2(\rho_p - \rho_L)r\omega^2}{9\eta}\left(1 - e^{\frac{-9\eta t}{2a^2\rho_s}}\right) \quad (5)$$

For the limit of $t \to \infty$, velocity v is given by

$$v_\infty = \frac{2a^2(\rho_p - \rho_L)r\omega^2}{9\eta} \quad (6)$$

In a multiphase system, the particle velocity can be described as follows [14]:

$$\sum_{i=1}^{n} v_i\phi_i + v_L(1 - \phi_{tot}) = 0 \quad (7)$$

The velocity of the liquid v_L is in the opposite direction to the velocity of the fastest particle. If transport by ordinary diffusion [15] is neglected, the relative velocity of particles and liquid $v_i - v_L$ can be based on the particle velocity for infinite dilution $v_{\infty,i}$, as given by Stokes' Law for the creeping flow regime. In a multiphase system, Eq. 6 is transformed as follows:

$$v_{\infty,i} = \frac{2r_{p,i}^2(\rho_{p,i} - \rho_L)r\omega^2}{9\eta} \quad (8)$$

where $r_{p,i}$ is the radius of i-type particle, $\rho_{p,i}$ is the density of i-type particle.

A correction to the particle–liquid slip velocity considering the effect of a higher suspension concentration is carried out through the hindrance factor $h_i(\varphi_{tot})$ [16]:

$$v_i - v_L = v_{\infty,i}\frac{\rho_{p,i} - \rho_s}{\rho_{p,i} - \rho_L}h_i(\phi_{tot}) \quad (9)$$

The suspension density ρ_s is given by

$$\rho_s = (1 - \phi_{tot})\rho_L + \sum_{i=1}^{n}\phi_i\rho_{p,i} \quad (10)$$

The hindrance factor h_i (φ_{tot}) is given by [13]

$$h_i(\phi_{tot}) = (1 - \phi_{tot})^{n_i - 2} \quad (11)$$

where ϕ_{tot} is the total solid content of Al_2O_3–ZrO_2 slurries, ϕ_i is the solid content of i-type particle in the slurries. The value of n_i is a function of the Reynolds number and the particle to vessel size ratio [13]. For a system with low Reynolds number and negligible wall effects, $n_i = 4.65$ [13]. The particle velocity in the multiphase system v_i is given by combining Eqs. 7–11

$$v_i = \frac{2}{9\eta}[r_{p,i}^2(\rho_{p,i} - \rho_s) - \sum_{j=1}^{n} r_{p,j}^2(\rho_{p,j} - \rho_s)\phi_j](1 - \phi_{tot})^{n_i - 2}r\omega^2 \quad (12)$$

Equation 12 was adopted to analyze the segregation phenomena in Al_2O_3–15 vol.%ZrO_2 system. In the slurries

with 50 vol.% solid content, the settling velocities of Al_2O_3 and ZrO_2 particles were calculated with the data from Table 2 and Eq. 12. They were 3.75 and 4.39 μm/s, respectively. The velocities of two kinds of particles are very close and both in the range of several μm/s, which also demonstrates segregation can be hindered at high enough solid contents. However, Chang et al. [10] reported a severe segregation between Al_2O_3 and ZrO_2 particles for 20 vol.% slurry of Al_2O_3–30 vol.%ZrO_2 composite. Their settling velocities were recalculated using the data from the Table 3 and Eq. 12. The result indicated settling velocities of Al_2O_3 and ZrO_2 particles were 25.7 and 147.9 μm/s, respectively. The velocity difference of two kinds of particles in Chang et al.'s study was much larger than that in our research, which was mainly attributed to the differences of solid contents and particle sizes of Al_2O_3 and ZrO_2 in two different slurries. The higher solid contents in the former helped to hinder severe segregation. In addition, it is seen in Eq. 12 that the settling velocities of particles primarily depend on r_p^2 $(\rho_p - \rho_s)$. In this study, the radius of higher density ZrO_2 particles was smaller than lower density Al_2O_3 particles, which made the above difference decrease. But in Chang et al.'s system the situation was opposite and the difference was increased. As pointed out by Biesheuvel and Verweij [11], Eq.12 also indicate a change in ω or η can influence the particle velocities to the same extent and can't influence the cast profile though the necessary time forming compacts is affected.

Drying and sintering behavior

After centrifugation, the supernatant water was removed. However, the centrifuged green bodies still contained 9 wt.% to 11wt.% water, which evaporated during dying. It is well known that fast evaporation of the liquid can lead to the formation of cracks in the green body and decrease of mechanical properties in the sintered body. So centrifuged compacts were slowly dried in low temperature and moist environment. Linear shrinkage during drying was about 1.0% for compacts prepared from high-solids-content slurries.

Dried samples were heated to 550 °C at a low rate of 1 °C/min and then sintered to 1,550 °C at a rate of 5 °C/min. This is because EPS spheres decompose from 300 to 550 °C according TG–DTG curve shown in Fig. 5. During this period, low heating rate contributes to EPS spheres slowly decompose and volatilize decreasing the drawbacks to keep samples integrity.

Solid contents of slurries can affect shrinkage of sintered compacts. A compact made from the slurry with low solid loading (30 vol.%) showed different shrinkage behavior at the top and bottom. Shrinkage of the top (18.3%) was more than that of the bottom (13.6%). This is because low solid content can't hinder preferential sedimentation of larger particles and induce obvious mass segregation in the compact. The top was composed of finer particles and finer pores than the bottom. According to the difference in sintering kinetics of smaller and larger particles, the top shows faster sintering behavior and bigger shrinkage than the bottom [15]. This difference became negligible for compacts made from slurries with high solid loading (50 vol.%). The top and bottom showed identical shrinkage (13.2%) over the whole sample. The cell struts in sintered products had uniform density of about 99.1%TD.

Table 3 Parameters and data used by Chang et al.

Parameter	Value
r	0.1016 m
ω	354 rad/s
d_1	0.2 μm
d_2	0.3 μm
η	1.0×10^{-3} pa s
ρ_1	3,940 kg/m^3
ρ_2	6,050 kg/m^3
ρ_L	1,000 kg/m^3
$n_1 = n_2$	4.65

Microstructure and macrostructure

A picture of partial open-cell Al_2O_3-ZrO_2 ceramic foams obtained from this work is shown in Fig. 6. The mean cell size is about 1.2 mm and cell structure is approximately uniformly arrayed. The difference of cell size mainly originates from the initial EPS spheres so if the spheres are further strictly sieved Al_2O_3–ZrO_2 foams with the same cell size can be obtained. In addition, the cell size of final products can be adjusted by changing the size of EPS spheres (several hundred μm to several mm).

In this paper, EPS spheres are compressed into dense packing at applied loads varying from 1,250 to 2,000 g because of their deformable nature. There is some asymmetrical deformation during compressing process, but the deformation is within the tolerable degree in our research, because the compressible properties of EPS spheres are experimented to avoid excessive compression deformation before choosing the range of applied loads. Figure 7 shows the micrograph of the pore of the sintered specimen prepared with the template at the applied load of 2,000 g. In Fig. 7, the ratio of pore diameter in along and perpendicular to the compression direction is about 0.9, and the pore is approximate to sphere shaper rather than to a pancake. Additionally, the influence of pore asymmetry on compressive property of sintered Al_2O_3–ZrO_2 foams is

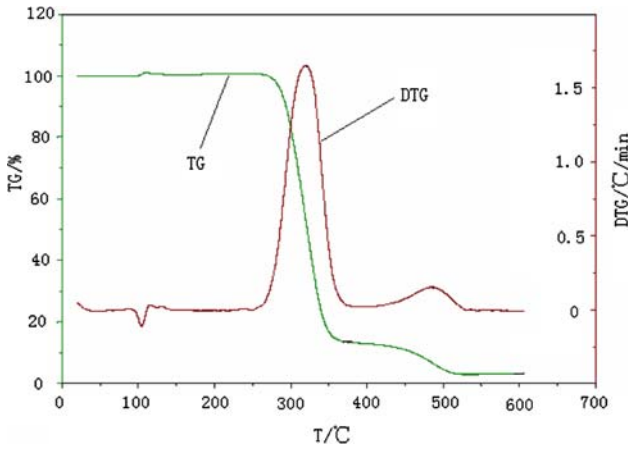

Fig. 5 TG and DTG curves of EPS spheres at a heating rate of 10 °C/min

approximately ignored in this paper due to the pore deformation within the tolerable degree.

It has been demonstrated that the segregation of Al_2O_3 particles can be hindered at slurries with 50 vol.% solid content in our previous research, which is consistent with the study of Huisman [17]. In this study, the segregation of ZrO_2 particles was mainly investigated. Figure 8 shows BSE micrograph of cell struts in top and bottom of cakes prepared by slurries with 50 vol.% solid content. As can be seen in Fig. 8, the ZrO_2 particle distribution in the top and bottom is homogeneous and there is no significant segregation phenomenon. The mean grain size measured is 340 and 365 nm, respectively. Though the average grain size of the top is slightly smaller than that of the bottom, it is within the tolerable degree. It indicates preferential settlement of ZrO_2 particle can be hindered at enough high solid content (>50 vol.%).

Porosity and compressive strength

Porosity (P) of ceramic foams can be calculated using Eq. 13 [18]:

$$P = 1 - (\rho_a/\rho_r) \tag{13}$$

where ρ_a is apparent density determined as the ratio of mass to volume and ρ_r is the real density of cell struts.

In this paper, the porosity of sintered samples can be adjusted by changing the weight placed on the top of the template during packing. Table 4 shows the effect of the applied load on porosity and compressive strength of sintered products. As can be seen in Table 4, the porosity can increase from 75.3% to 83.1% with the varying of the applied load from 1,250 to 2,000 g. This is mainly due to the deformable nature of EPS spheres. These spheres are compressed into dense packing at high additional load, improving interactional area of EPS spheres and decreasing the porosity of the template. Contrarily, the porosity of final products increases. At present, the adjustment of the porosity has been further studied. In Table 4, the compressive strength of sintered products decreases from 3.82 to 2.07 MPa with the increase of the porosity because of the reduction of effect area to support load.

For commercial Al_2O_3 matrix foams, the applied benchmark of compressive strength is 0.8 MPa. Additionally, in Han et al's study [19], the compressive strength of Al_2O_3 foam is 1.3 MPa at the porosity of 86%. So our experimental results (2.07–3.82 MPa) shows Al_2O_3–ZrO_2 foams have a high crushing strength that is sufficient for metal filtration. In this study, the higher compressive strength of Al_2O_3–ZrO_2 foams came form the dense cell struts with higher density and less holes and cracks. Additionally, uniform cell structure also contributes to

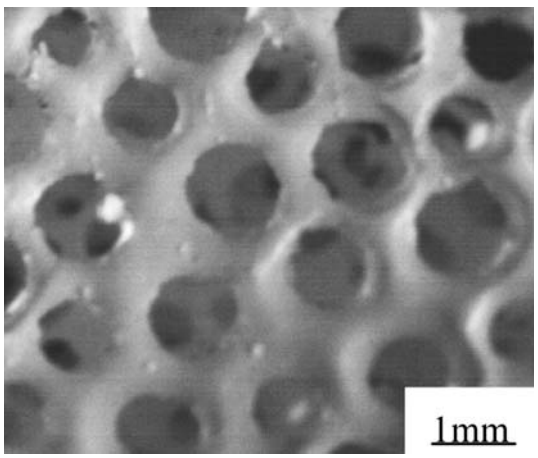

Fig. 6 Macrostructure of the porous Al_2O_3–ZrO_2 foam

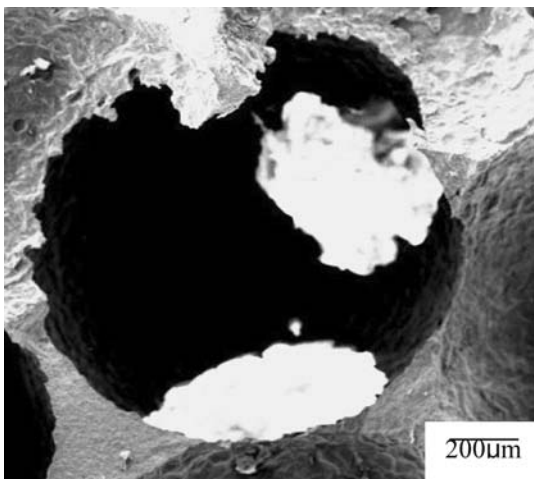

Fig. 7 Microstructure of the pore of Al_2O_3–ZrO_2 foam

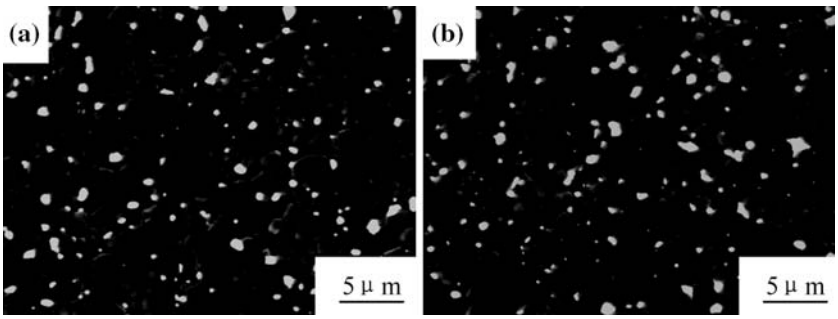

Fig. 8 Microstructures of cell struts in the Al_2O_3–ZrO_2 foam prepared from the slurry of 50 vol.% solid content (BSE) (**a**) top surface; (**b**) bottom surface

Table 4 Porosity and compressive strength of Al_2O_3–ZrO_2 foam at different applied loads

Applied load (g)	Porosity (%)	Compressive strength (MPa)
1,250	75.3	3.82
1,500	77.2	3.38
1,750	79.8	2.81
2,000	83.1	2.07

decrease stress concentration and preferential fracture derived from weaker columns.

Conclusion

A novel process was reported here to prepare Al_2O_3–ZrO_2 ceramic foams with controlled cell structure. It utilized EPS spheres to array ordered templates and centrifugal slip casting to obtain cell struts with high packing density. This method can avoid holds and cracks formed by the pyrolysis of organic sponges. The sintered Al_2O_3–ZrO_2 foams had dense cell struts, uniform cell structure and a high crushing strength that is sufficient for metal filtration. Changing the diameter of EPS spheres and the loads applied on them during packing can adjust the cell size and porosity of the products, respectively. In centrifugal process, segregation phenomenon mainly came from the difference of settling velocity of different particles. Slurries with high solid contents (> 50 vol.%) can hinder obvious mass segregation and the cell struts in the cakes had high green (61.5%TD) and sintered density (99.1%TD) as well as homogeneous microstructure. Due to the deformable nature of EPS spheres, the porosity of sintered compacts increased from 75.3% to 83.1% with the applied load varying in the range of 1,250 to 2,000 g. Their compressive strength decreased from 3.82 to 2.07 MPa with the increase of the porosity because of the reduction of effect area to support load.

Acknowledgements This work was supported partly by the National Natural Science Foundation of China (50672014) and the National Science Fund for Distinguished Young Scholars (50425413).

References

1. Yang SM, Coombs N, Geoffery A (2000) Adv Mater 12:1940
2. Strom LA, Sweeting TB, Norris DA, et al (1995) Mater Res Soc Symp Proc 371:321
3. Montanaro L, Jorand Y, Fantozzi G, et al (1998) J Eur Ceram Soc 18:1339
4. Zhang Y (2004) Mater Res Bull 39:755
5. Powell SJ, Evans JRG (1995) Mater Manuf Process 10:757
6. Brezny R, Green DJ (1989) J Am Ceram Soc 72:1145
7. Hargus PM, Mula JA, Redden MK (1989) US Patent 4866011
8. Lee Byong-Taek, Lee Kap-Ho, Hiraga Kenji (1998) Scr Mater 38:1101
9. Lange FF (1989) J Am Ceram Soc 72:3
10. Chang JC, Velamakanni BV, Lange FF, et al (1991) J Am Ceram Soc 74:2201
11. BergstrÖm L, Schilling CH, Aksay IA (1992) J Am Ceram Soc 75:3305
12. Biesheuvel PB, Verweij H (2000) J Am Ceram Soc 83:743
13. Wallis GB (1969) One-dimensional two-phase flow. McGraw-Hill, New York
14. Lockett MJ, Al-Habbooby HM (1974) Powder Technol 10:67
15. Bird RB, Stewart WE, Lightfoot EN (1960) Transport phenomena. Wiley, New York
16. Masliyah JH (1979) Chem Eng Sci 34:1166
17. Huisman W, Graule T, Gauckler LJ (1995) J Eur Ceram Soc 15:811
18. Moreira EA, Innocentini MDM, Coury JR (2004) J Eur Ceram Soc 24:3209
19. Han Y-s, Li J-b, Wei Q-m et al (2002) Ceramics international 28:755